JOURNAL OF GEOPHYSICAL RESEARCH, VOL. 105, NO. A2, PAGES 2315-2324, FEBRUARY 1, 2000

The solar magnetic field and the solar wind: Existence of preferred longitudes

M. Neugebauer, E. J. Smith, A. Ruzmaikin, J. Feynman, and A. H. Vaughan
Jet Propulsion Laboratory, California Institute of Technology, Pasadena

Abstract. Direct measurements of the solar wind speed and the radial component of the interplanetary magnetic field acquired over more than three solar cycles are used to search for signatures of a persistent dependence of solar wind properties on solar longitude. Two methods of analysis are used. One finds the rotation period that maximizes the amplitude of longitudinal variations of both interplanetary and near-Earth data mapped to the Sun. The other is based on power spectra of near-Earth and near-Venus data. The two methods give the same result. Preferred-longitude effects are found for a synodic solar rotation period of 27.03 ± 0.02 days. Such high precision is attained by using several hundred thousand hourly averages of the solar wind speed and magnetic field. The 27.03-day periodicity is dominant only over long periods of time; other periodicities are often more prominent for shorter intervals such as a single solar cycle or less. The 27.03-day signal is stronger and more consistent in the magnetic field than in the solar wind speed and is stronger for intervals of high and declining solar activity than for intervals of low or rising activity. On average, solar magnetic field lines in the ecliptic plane point outward on one side of the Sun and inward on the other, reversing direction approximately every 11 years while maintaining the same phase. The data are consistent with a model in which the solar magnetic dipole returns to the same longitude after each reversal.

1. Introduction

A considerable body of evidence that recurrent solar activity is associated with specific solar longitudes has accumulated over the years. *Trotter and Billings* [1962] discerned a longitudinal persistence of solar active regions over one solar cycle, but not from one cycle to the next. *Bumba and Howard* [1969] demonstrated rigid rotation of low-latitude (±20°) patterns in the solar magnetic field which persisted for several months. On a longer timescale, *Bogart* [1982] found a persistence of 27-day modulations of daily sunspot numbers over a period of 128 years, consistent with long-lived active longitudes. This periodicity was found to be strong in some solar cycles and weak in others, however, and no attempt was made to compare the phases of sunspot variations in cycles for which the periodicity was present.

There have also been a number of studies of periodicities in the properties of the solar wind. With the first extended observations of the solar wind, *Snyder et al.* [1963] discerned a 27-day recurrence of high-speed streams over the 4-month period of observation. Using all near-Earth solar wind data obtained from 1964 to 1994, *Mursula and Zieger* [1996] found a ~27-day recurrence in the plasma speed, temperature, and density, in the interplanetary magnetic field, as well as in a number of solar parameters. Because they divided the data into sliding 512-day intervals, and then averaged the resulting power spectra, their results do not address the question of long-term persistence of preferred longitudes. Studies of variations in the solar wind speed over intervals of 3 [*Gosling and Bame*, 1972] and 11 years [*Fenimore et al.*, 1978] revealed that the recurrence period was not a steady 27 days but varied between 27 and 29 days from year to year and sometimes on even shorter scales. Using geomagnetic activity over the interval 1868-1983 as a proxy for solar wind speed, *Sargent* [1985] found multiyear periods of 27-day recurrence at the end of each sunspot cycle with the recurrence abruptly disappearing at the start of each new sunspot cycle. He did not investigate the phase stability over periods longer than 54 days. On the other hand, *Gosling et al.* [1977] found evidence for persistent preferred longitudes for the origins of high- and low-speed streams over the entire 11.5-year interval July 1964 to December 1975; the most pronounced longitudinal modulation was obtained for an assumed synodic rotation period of 27.025 days.

Solar rotation effects have also been sought in the interplanetary magnetic field (IMF), principally in its polarity. With early direct measurements of the IMF, *Wilcox and Ness* [1965] discovered a persistent polarity pattern which they named the "sector structure"; it corotated with the Sun, with a period of ~27 days, over three rotation periods. Later, *Wilcox and Colburn* [1970] found rotation periods ranging between 27 and 28 days for the interval 1963 through 1968. *Gonzalez and Gonzalez* [1987] combined direct measurements of the field polarity with polarities deduced from polar-region geomagnetic data for the period 1926-1982. Using data series either 500 days or 1 year in length, they found an over-all recurrence period of 27.5 days, but with year-to-year variations of the period between 27 and 28 days. The only study to focus on long-term stability of the IMF was that of *Svalgaard and Wilcox* [1975]. From the polarity of the IMF deduced from ground-based data over the years 1926-1973, they concluded that the longtudinal structure of IMF polarity persisted over five solar cycles with a period close to 27 days. Their results are compared to the results of the present study in greater detail in section 6.

Paper number 1999JA000298.
0148-0227/00/1999JA000298$09.00

In this paper we address the question of whether, despite the highly variable character of the Sun, the many manifestations of its activity, and the apparent jitter in the rotation period of the properties of the solar wind, are there periodicities and preferred longitudes that persist from one sunspot cycle to another? The existence, or absence, of preferred solar longitudes over long periods of time would have implications for our understanding of natural dynamos and of solar and stellar activity. In the case of the Earth's magnetic field the nonaxisymmetric component of the secular variation can be resolved into two parts, one of which drifts in longitude with time and another which does not. There are also hints of preferred longitudes in Sun-like stars. Observations of stellar magnetic activity via monitoring of calcium II H and K emissions provides evidence that some stars have preferred longitudes that persist over several activity cycles [*Vaughan et al.*, 1981; *Vaughan*, 1984]; in some cases the preferred longitude appears to shift by ~180° (A. H. Vaughan and S. L. Baliunas, unpublished paper presented at IAU Colloquium no. 141, Beijing, China, September 1992).

The properties of the solar wind and the IMF have now been measured, with some interruptions, for 37 years. Motivated by earlier reports suggesting the reality of preferred solar longitudes and by current work on stellar activity, we here use a very large data base to extend previous analyses of time variations of the solar wind to cover a period of more than three solar cycles of direct measurements.

2. Data Sources

The study is based on hourly averages of the solar wind speed and the IMF observed near Earth and in interplanetary space over the period 1962 to 1998. The data were acquired from the National Space Science Data Center (NSSDC). Except for the Mariner 2 and Pioneer 6 and 7 data sets, the data are available in the Coordinated Heliospheric Observations (COHO) database. We converted the Mariner 2 and Pioneer 6 and 7 data supplied by NSSDC to the COHO format with the exception that the magnetic field data from Mariner 2 were not used because of the large uncertainty in the spacecraft magnetic field.

The following parameters are used from this COHO-formatted data base: t_{obs} is the time of observation converted to integer hours since the start of 1962; λ_{obs} is the spacecraft longitude in heliographic inertial (HGI) coordinates, which are Sun centered and inertially fixed with respect to an axis along the intersection of the ecliptic and solar equatorial planes; R_{obs} is heliocentric distance, in AU; V is the observed hourly averaged averaged solar wind speed in kilometers per second; and B_r is the radial component of the magnetic field in nanotesla, normalized to 1 AU by multiplying the measured value by R_{obs}^2.

The sources of data are listed in Table 1, together with the years of observation, the number of hours of speed data, and the number of hours with both speed and magnetic field data. Inaccuracies in mapping the solar wind back to the Sun are limited by using only data acquired at solar distances less than 3 AU. For Ulysses, only the data acquired during the in-ecliptic phase of the mission are used. The study is based on 334,763 hours of speed data and 246,834 hours of field data. Note that using interplanetary data in addition to the near-Earth OMNI data doubles the number of hourly averages available for analysis, thus providing precision not previously attained.

Table 1. Number of Hourly Averages of Solar Wind Parameters Used in Analysis

Source	Time Interval	V only	V and B
OMNI file	1963.9 - 1998.9	164,970	137,479
Mariner 2	1962.7 - 1962.9	1,429	0
Pioneer 6	1966.0 - 1967.7	3,258	3,258
Pioneer 7	1966.6 - 1967.8	2,841	2,841
Pioneer 10	1972.3 - 1972.9	4,041	3,919
Pioneer 11	1973.3 - 1974.0	5,028	4,145
Helios 1	1974.9 - 1981.0	42,458	24,329
Helios 2	1976.0 - 1980.2	26,472	14,015
Voyager 1	1977.7 - 1978.3	2,949	2,943
Voyager 2	1977.6 - 1978.4	4,137	4,120
Pioneer Venus Orb.	1978.9 - 1992.8	73,103	45,717
Ulysses	1990.0 - 1991.4	4,077	4,068
Total		334,763	246,834

OMNI data were included through November 30, 1998 (V) or September 30, 1998 (B). Interplanetary spacecraft data were used only for the interval when the spacecraft were less than 3 AU from the Sun.

3. Data Mapped Back to the Sun

For each hour of data the constant-speed, radial-flow approximation is used to map the solar wind from the spacecraft to the Sun and to determine the time the plasma left the Sun and the longitude of the source region. The time t_s when the solar wind left the Sun is given (in hours since the start of 1962) by

$$t_s = t_{obs} - 41556\, R_{obs}/V. \qquad (1)$$

Because the flow is assumed to be radially outward from the Sun in an inertial frame of reference, the longitude λ of the solar source, in HGI coordinates, is the same as the longitude at which the data are obtained:

$$\lambda \text{ (at time } t_s) = \lambda_{obs} \text{ (at time } t_{obs}). \qquad (2)$$

If λ_e is the HGI longitude of Earth at time t_s, then the difference in longitude between the solar wind source and the sub-Earth point is

$$\Delta\lambda = \lambda - \lambda_e. \qquad (3)$$

For this study we are interested in the solar longitude ϕ rather than in the inertial longitude λ. Solar longitude depends on two parameters: the solar rotation period P and a definition of the zero of longitude. The rotation period is determined by the data, as explained in the next paragraph. Zero longitude is arbitrarily defined to be the sub-Earth solar meridian at 0000 UT on January 1, 1962. For $P = 27$ days our solar longitude is related to the Bartels rotation used in the study of geomagnetic activity; for an average travel time of the solar wind from the Sun to the Earth of 4 days, each Bartels rotation would start at 253° in our longitude system.

The steps in the analysis are as follows: (1) A synodic solar rotation period P (e.g., P = 27.0 days) is assumed. (2) The solar longitude ϕ of a solar wind source region is then calculated from t_s and $\Delta\lambda$ as follows:

$$\tau = (t_s - t_o)/(24\, P), \qquad (4)$$

where τ is the number of rotations since time t_o = 0000 UT on January 1, 1962. The solar longitude of Earth, in degrees, is

$$\phi_e = 360° \times (\text{the fractional part of } \tau = \text{mod}(\tau, 1.0)) \quad (5)$$

and the solar longitude of the solar wind source region is then

$$\phi = \phi_e - \Delta\lambda. \quad (6)$$

The integer part of τ provides a rotation counter. (3) The solar wind speed V and the normalized radial component of the field B_r are then binned according to the values of τ and ϕ. The τ bins are one solar rotation in duration, and the ϕ bins are 10° wide. The longitudinal resolution of 10° is chosen to match the approximate accuracy of the mapping procedure [*Nolte and Roelof*, 1973]. (4) After all the data from all the spacecraft are mapped back, average values of V and B_r are calculated for each bin to obtain two matrices, each with 36 columns (longitudes) and ~500 rows (solar rotations). The precise number of rows depends on the rotation period. (5) Each column of the speed

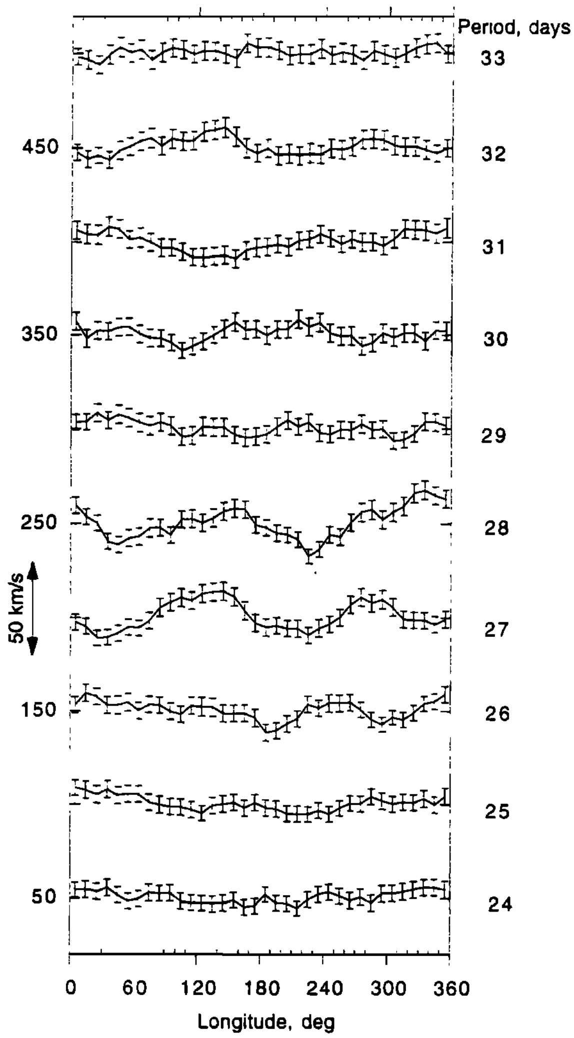

Figure 1. Time-averaged variations of solar wind speed versus solar longitude for 10 assumed values of the solar rotation period (given on the right). The tick marks on the left and right scales for each trace represent a speed of 450 km/s. The error bars indicate probable errors calculated from the spread of values in each longitude column in the time-longitude matrix described in the text.

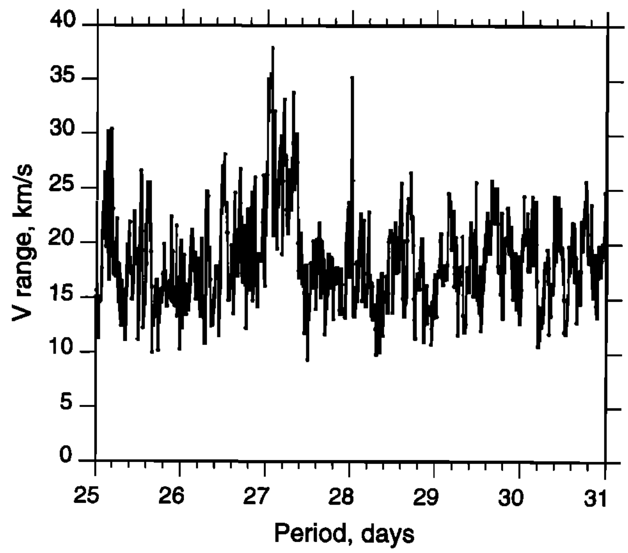

Figure 2. The difference between the highest and the lowest speeds for the time-averaged speed versus longitude curves as a function of solar rotation period from 25 to 31 days.

matrix is averaged to yield time-averaged speed versus longitude. (6) Steps 1 through 5 are repeated for a number of different rotation periods.

Time-averaged longitudinal speed profiles are shown for 10 different rotation periods between 24 and 33 days in Figure 1. The longitudinal modulation of the speed is flat, within the probable-error bars, for periods of 24, 25, 32, and 33 days. The greatest longitudinal modulations appear at 27 and 28 days. Figure 2 shows the results for trial periods separated by 0.01 days, where the abscissa is the assumed period and the ordinate is the speed range, which is the amplitude (peak to minimum) of the speed variation with longitude. The largest amplitude variation occurs at a period slightly greater than 27 days. For periods between 27.01 and 27.05 days the speed range exceeds the range of all the other peaks.

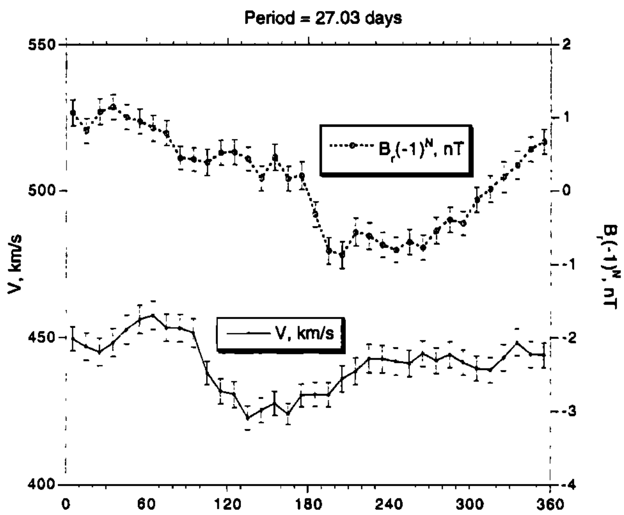

Figure 3. The time-averaged speed (V) and radial field ($B_r(-1)^N$) versus longitude for a rotation period of 27.03 days.

Table 2. Definition of Solar Cycles Used to Average the Solar Wind Data and the Number of Hourly Values in Each Interval

Cycle	Years Included	Sign of B_r	No. of V Points	No. of B_r Points
A	1962.10 to 1966.74	as measured	14,066	6,877
B	1966.74 to 1977.54	reversed	107,481	78,618
C	1977.54 to 1988.34	as measured	159,721	122,012
D	1988.38 to 1998.75	reversed	60,296	39,327

The statistical significance of the preferred longitudes evaluated in this way can be judged by the longitudinal profile for a period of 27.03 days shown in Figure 3. The speed profile is the lower of the two curves. The error bars denote probable errors (standard deviation divided by the square root of the number of points). The maximum value of the speed exceeds the minimum value by 8 times the average probable error. Furthermore, the values of the speed are not randomly distributed in longitude. The average of the points in Figure 3 is 441 km/s and their standard deviation is 9 km/s. Rather than high and low values of V being distributed randomly in longitude, there are six consecutive points (15° - 95°) more than one standard deviation above the average and nine consecutive points (115° - 195°) more than one standard deviation below the average.

Analysis of the mapped-back values of B_r is complicated by the polarity reversal of the solar magnetic field approximately every 11 years; any longitudinal variation of B_r would be washed out in grand averages over the entire period of analysis as was done for the speed in Figures 1 - 3. A contour plot (not shown) of the longitude-time matrix for the field data for P = 27.03 days suggests that the reversal of the in-ecliptic IMF occurs neither near solar maximum, when the solar surface field reverses, nor near solar minimum, but during times of increasing solar activity.

A more quantitative estimate of the time of reversal of the IMF is obtained by first smoothing the data in the longitude-time B_r matrix by taking five-point running averages in each dimension, and then fitting the value of B_r in every second longitude and every second time bin to a function of the form

$$B_r = B_{ro} \sin(\phi - \phi_o) \sin(\theta - \theta_o) \tag{7}$$

$$\theta = 360° \tau/292 \tag{8}$$

where B_r and ϕ are values from the smoothed matrix and the factor 292 in (8) is the number of 27.03-day rotations in a 21.6-year solar magnetic cycle (an average cycle length for the years 1954-1996). The unknowns B_{ro}, ϕ_o, and θ_o are solved for by least squares. The result is B_{ro} = 1.35 nT, ϕ_o = 328°, and θ_o = 259°. This value of θ_o corresponds to reversals of the IMF at years 1966.74 + 10.8N, where N = 0, 1, 2, 3. We therefore define four solar cycles, called cycle A through cycle D as summarized in Table 2, and change the sign of B_r for cycles B and D. In all further calculations involving the magnetic field, we use the parameter $B_r(-1)^N$; the sign change is equivalent to a 180° phase shift of B_r in alternate cycles.

The relation of our cycles A-D to the sunspot cycle is shown in Figure 4. The sunspot data are monthly averages obtained from http://ftp.ngdc.noaa.gov/stp/solar_data/. The sign reversal occurs during the rising phase of the solar activity cycle slightly before solar maximum. This is, of course, only a simple approximation to the complex reversals of the solar magnetic field. It is perhaps interesting to note that this change of sign of the in-ecliptic magnetic field occurs more than a year before the reversals of the solar polar magnetic fields.

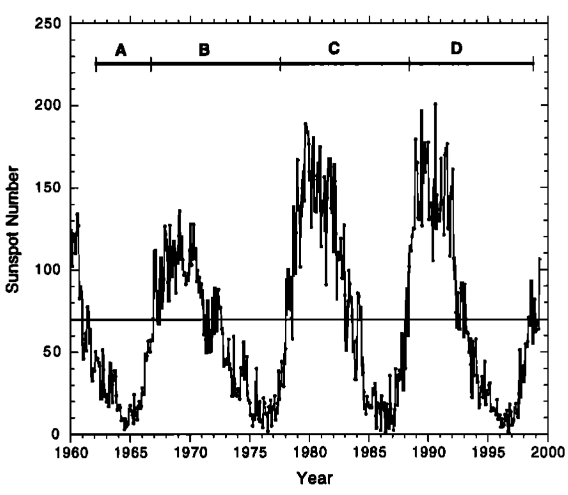

Figure 4. Monthly averaged sunspot numbers for the past 40 years. The start and stop times of our cycles A-D, when the sign of B_r is reversed, are shown at the top.

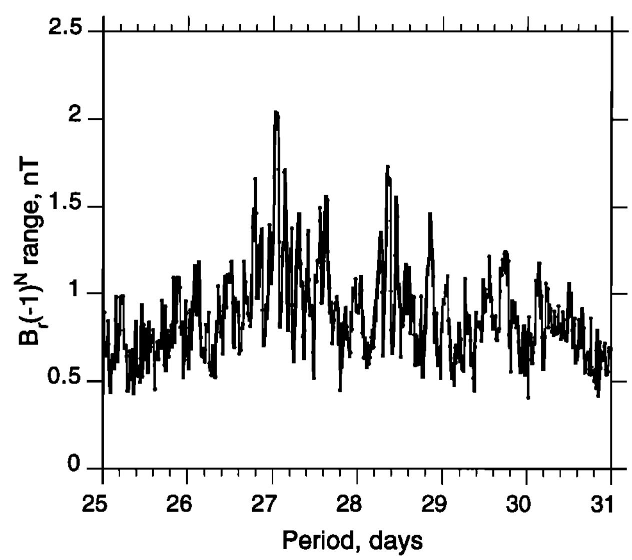

Figure 5. The difference between the highest and the lowest values of $B_r(-1)^N$ for the time-averaged $B_r(-1)^N$ versus longitude curves as a function of solar rotation period from 25 to 31 days.

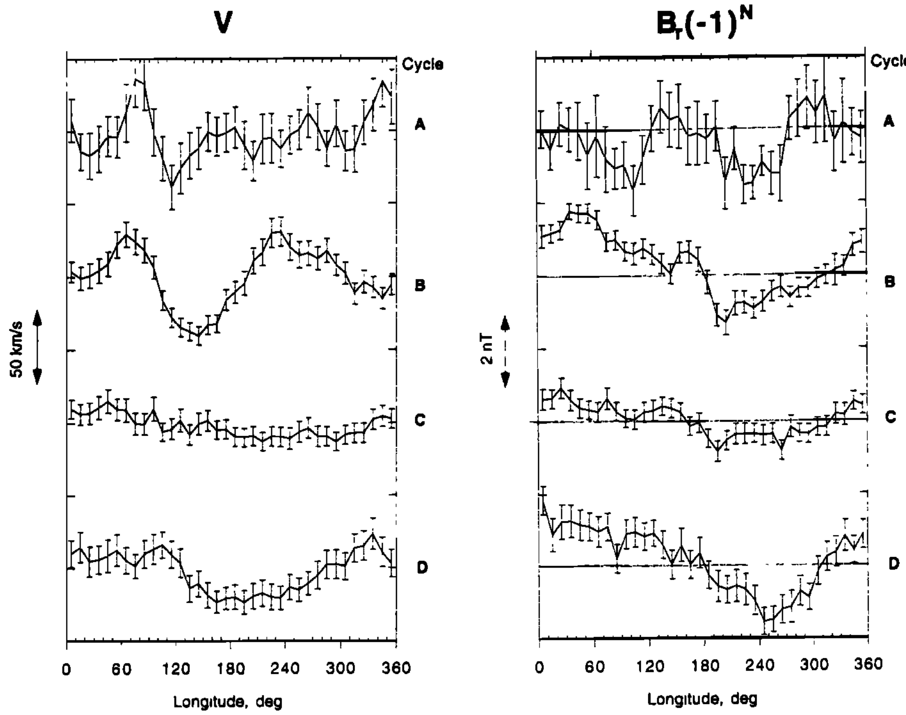

Figure 6. Time-averaged profiles of V and $B_r(-1)^N$ versus longitude for a solar rotation period of 27.03 days, given separately for cycles A-D. The horizontal lines in the right-hand panel indicate $B_r(-1)^N = 0$ nT.

With this change of sign in alternate cycles the field data are then processed in the same way as the speed data, resulting in Figure 5. The highest peak in Figure 5 extends from 27.01 to 27.06 days, in agreement with the speed data. The statistical significance of the longitudinal variation at 27.03 days can be judged from the upper curve in Figure 3. The maximum exceeds the minimum by >11 times the average probable error, and there are 7 (9) consecutive points more than one standard deviation above (below) the average value. For the field data the second highest peak is at 28.27 days, which differs from the 28.0-day secondary peak seen in Figure 2 for the speed data.

An important question is whether the longitudinal variation associated with a period of 27.03 days persists over all 37 years or whether the amplitudes of the variations in specific cycles, e.g., 1964-1975, are so large that they dominate the variation for the entire period. This question is addressed by analyzing the data for each cycle separately. Figure 6 shows time-averaged V and B_r $(-1)^N$ versus longitude for a rotation period of 27.03 days for cycles A through D. Although there are speed maxima at ~60° longitude in each cycle, the speed profiles exhibit great variation from one cycle to the next, with cycle B having two peaks, cycle C having very little modulation, and cycle D being intermediate between cycles B and C. Except for cycle A, for which there is very little field data, the magnetic field does exhibit cycle-to-cycle regularity, with maxima at ~30° and minima between 200° and 250° in each cycle.

The plots for cycle B are a good illustration of the Earth encountering two high-speed streams with opposite magnetic polarities per solar rotation. Such a topology is often encountered during periods of declining solar activity when the Sun has large polar coronal holes which reach down to low latitudes due to the tilt of the solar magnetic dipole [e.g., *Hundhausen*, 1977]. The high-speed wind from the northern polar coronal hole has the opposite magnetic polarity than the high-speed wind from the southern polar coronal hole which is observed half a rotation later.

The range versus period plots similar to Figures 2 and 5 are shown for each cycle in Figure 7. For reference, the dashed lines indicate a period of 27.03 days. The speed data for cycle C show little modulation at any period, whereas there is a peak near 27.03 days for cycles A, B, and D, although it is not always the largest peak. For the field data, there is a peak near 27.03 days for cycles B, C, and D, but a minimum at that period for cycle A for which there is very little field data.

4. Analysis of Time Series Data

The speed and field variations can also be analyzed as simple time series rather than as longitude-time matrices. It is not, however, possible to combine the interplanetary data with the near-Earth data for this type of analysis because corotating the interplanetary data to Earth requires knowledge of the solar rotation period, which is the unknown parameter we are trying to find. We are thus limited to using the OMNI data set for which the statistics of data coverage are given in Table 3. Because we are interested only in periodicities in the neighborhood of 27 days, we decrease the computational time and increase the percent data coverage by forming 12-hour averages of V and B_r. The data coverage is still rather poor, with 35.6% and 34.9% gaps in the speed and field data, respectively. Because of the large fraction of missing data, we use the Lomb-Scargle periodogram method [*Press et al.*, 1992] of computing spectral power as a function of frequency or period.

Figure 8 shows the periodograms of V and $B_r(-1)^N$ from the OMNI data. Both panels show power enhancements near pe-

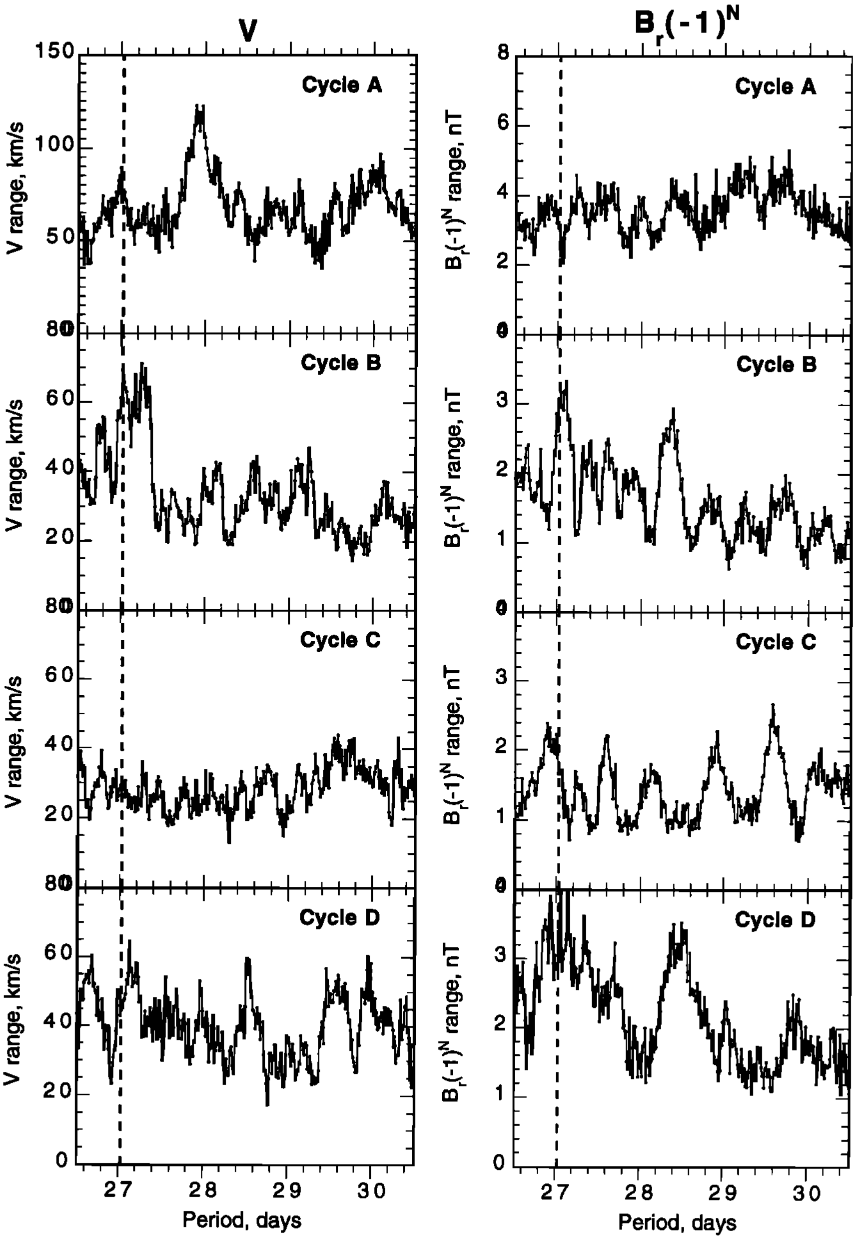

Figure 7. The same as Figures 2 and 4, but given separately for cycles A-D. The dashed line indicates a period of 27.03 days.

riods of 13.5 days, 27 days, and 1 year. *Fenimore et al.* [1978] previously showed that there is frequently more power in the solar wind speed spectrum at 13.5 days than at 27 days. *Mursula and Zieger* [1996] studied the 13.5-day periodicity of the solar wind and interplanetary magnetic field in greater detail and found that it is most prominent during solar cycle phases when the Earth encounters two high-speed streams per solar rotation. The peaks near one year are probably a latitudinal dependence of V and B_r caused by the annual variation of the heliographic latitude of the Earth. The highest peak in the speed periodogram falls at 9.38 years, which is near, but somewhat less than the 10.8-year periodicity in the sunspot cycle. Changing the sign of B_r in alternate cycles leads to the disappearance of a peak at ~22 years for that parameter.

Table 3. Statistics of the OMNI Data Set Used in the Time Series Analysis

	V	B_r
Number of hours covered	306,897	305,386
Number of hourly averages	164,791 (53.7%)	169,962 (55.7%)
12-hour averages in cycle A	989	618
12-hour averages in cycle B	5785	6226
12-hour averages in cycle C	5651	5746
12-hour averages in cycle D	4066	3972
Total	16,491 (64.4%)	16,562 (65.1%)

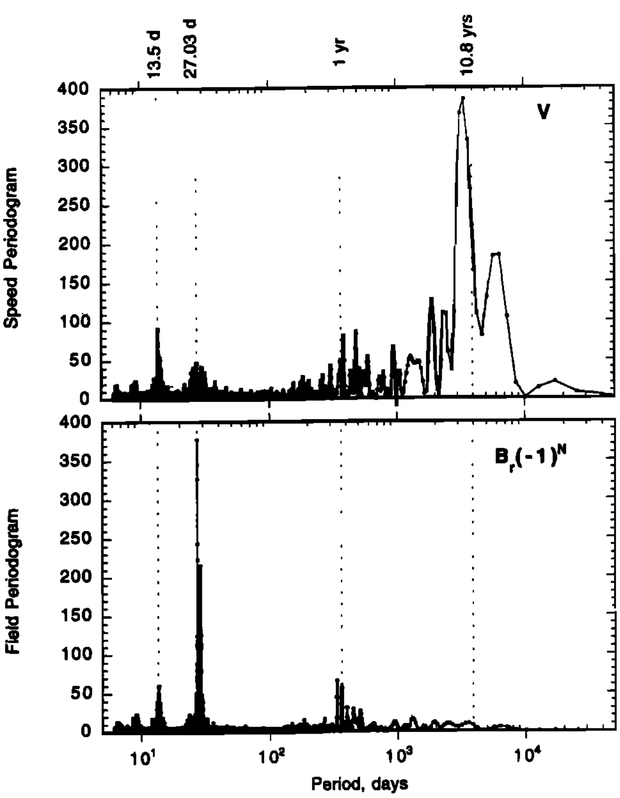

Figure 8. Lomb-Scargle periodograms calculated from 12-hour averages of hourly averages of V and $B_r(-1)^N$ in the OMNI database.

The peaks near 27 days are shown at higher resolution in Figure 9. Both V and $B_r(-1)^N$ have strong maxima in their periodograms near 27.03 days, which is indicated by the vertical line, thus confirming the results found in the previous section (Figures 2 and 5).

Press et al. [1992] provide an estimate of the probability that a periodogram peak of height z is the result of random noise rather than a true periodic signal. For the V and $B_r(-1)^N$ periodogram peak heights shown in Figure 9, their algorithm gives formal null hypothesis probabilities of 10^{-17} and 10^{-161}, respectively. *Hernandez* [1999] argues that the null hypothesis probability should be calculated from the half height $z/2$, rather than from z, which would yield null probabilities of $10^{-6.5}$ and 10^{-79}, which are still remarkably small numbers.

The periodogram method can give spurious peaks when the data stream contains periodic data gaps, and there are also questions concerning the number of independent frequencies or degrees of freedom that enter the calculation of probabilities [*Horne and Baliunas*, 1986; *Hernandez*, 1999]. We therefore compute periodograms for a series of Gaussian random numbers with variances equal to the observed variances of V and $B_r(-1)^N$ sampled at the same unevenly spaced times as the observations. The resulting periodograms are also plotted in Figure 9 as the lines without data points on them. There is very little power in the periodograms derived from the random data. The 27.03-day peak in the V periodogram in Figure 9 is 5.6 times higher than the highest peak in the random-V periodogram, indicating at least a 5-σ result. A similar analysis for the field data shows that the 27.03-day periodicity in $B_r(-1)^N$ is significant at the 29-σ level or more. Note that neither random periodogram has a peak at 27.03 days. We conclude that false peaks due to periodic gaps are not a concern.

Of the spacecraft well removed from Earth and not contributing to the OMNI data set, only Pioneer Venus Orbiter (PVO) provides a good opportunity for time series analysis. The PVO magnetometer data set runs nearly 10 years from December 1978 to August 1988, and thus nearly coincides with our cycle C. The fractional coverage of 12-hour averages of the magnetic field observed at PVO is 0.713. A periodogram is calculated as a function of the period P_v observed at Venus and the result is then transformed to the period P_e which would be observed if the spacecraft were at Earth. It can be shown that

$$1/P_v + 1/Y_v = 1/P_e + 1/Y_e, \tag{9}$$

where Y_v = 224.701 days and Y_e = 365.256 days are the lengths of the Venusian and terrestrial years, respectively. The resulting periodogram of $B_r(-1)^N$ observed at Venus versus P_e is shown in Figure 10 together with the nearly simultaneous periodogram obtained from the OMNI data for cycle C. The two periodograms have peaks at nearly the same values of P_e, with the PVO data have a higher (more significant) peak near 27 days than the OMNI data. This peak is centered at a period slightly less than 27 days, consistent with the cycle C data shown on the right side of Figure 7.

5. Dependence on Solar-Cycle Phase

The analyses presented in the two previous sections are based on averages either over the entire duration of direct ob-

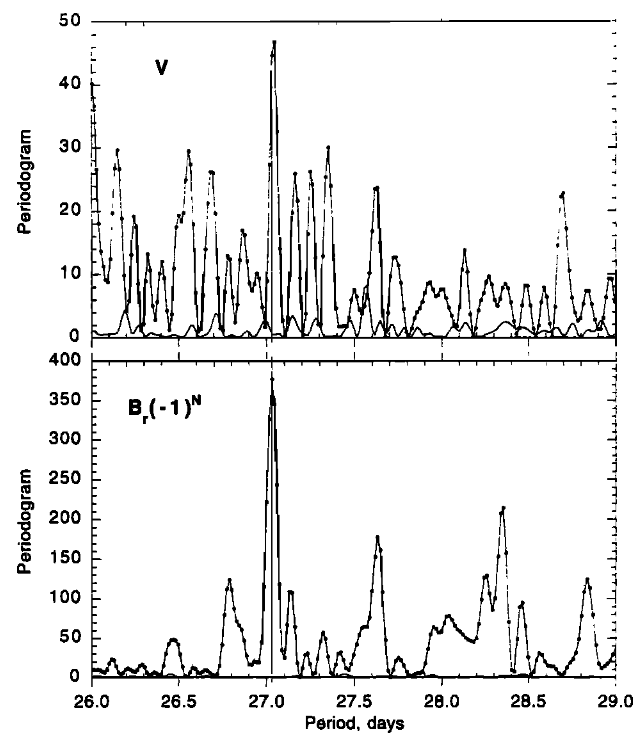

Figure 9. The same as Figure 8 with an expanded timescale for periods of 26 to 29 days. The lower curves, without data points, are the periodograms calculated for a random distribution of each parameter sampled at the same times as the data in the OMNI file.

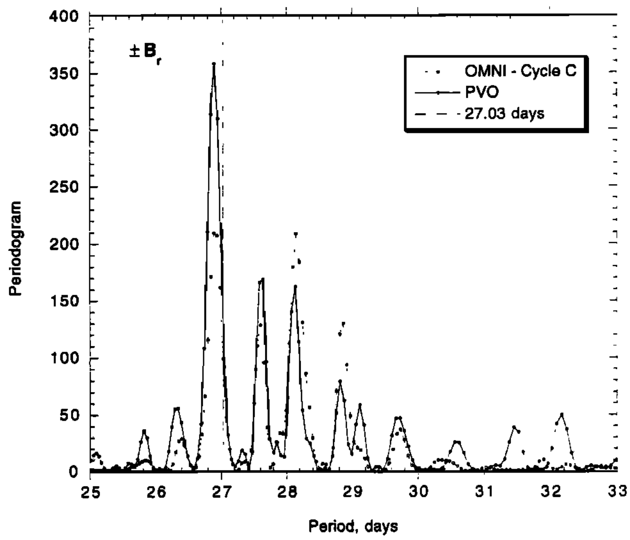

Figure 10. A periodogram of B_r calculated from 12-hour averages of Pioneer Venus Orbiter (PVO) data and comparison with the periodogram calculated from the OMNI data base for cycle C. The actual period observed at Venus has been shifted to the equivalent synodic period at Earth according to Equation 9. The vertical dashed line indicates a period of 27.03 days.

servations of the solar wind or over 10.8-year solar cycles. A remaining question is whether the presence of the periodicity of 27.03 days depends on the phase of the solar cycle. We choose a dividing line between sunspot maximum and sunspot minimum at a sunspot number of 70, indicated by the horizontal line in Figure 4. This particular value is chosen because it divides the data into two bins containing roughly the same number of data points. A period of maximum(minimum) activity is defined to start the first time the sunspot number exceeds (drops below) a value of 70. The lowest and highest monthly means for each cycle shown in Figure 4 are used to define the boundaries of intervals of rising and declining activity. Figure 11 shows periodograms of $B_r(-1)^N$ calculated separately for intervals of sunspot maximum and minimum and rising and declining activity. The highest peak is that at 27.03 days for $B_r(-1)^N$ at solar maximum. There is also a significant 27.03-day peak for periods of declining activity, but not at solar minimum or during the rise to maximum. Similar periodograms for the solar wind speed did not show a dominant 27.03-day peak for any of the individual activity phases.

6. Discussion and conclusions

The two independent methods of analysis, one based on maximizing the amplitude of longitudinal variations of both interplanetary and near-Earth data mapped to the Sun and the other based on power spectra of near-Earth and near-Venus data, give equivalent results. They yield a statistically significant long-term periodicity of 27.03 ± 0.02 days. Our results agree very closely with the 27.025-day periodicity of solar wind speed observed by *Gosling et al.* [1977] over the interval 1964-1975.

The stated uncertainty of ±0.02 days corresponds to the widths of the 27.03-day peaks in Figures 2 and 5. The full width at half maximum of the $B_r(-1)^N$ periodogram in Figure 9 is ±0.03 days. The precision is limited by the amount of data used, and less data are used in the periodogram analysis than in the method based on the amplitude of speed and field variations mapped back to the Sun.

Preferred longitudes and the rotation periods are interrelated. Longitude cannot be defined independent of rotation period. Furthermore, the uncertainty in the rotation rate can be use to place limits on the longitudinal drift of features in the solar wind speed and magnetic field. The change in solar longitude $\Delta\phi$ in a time span Δt is given by

$$\Delta\phi = 360° \, \Delta t / P \quad (10)$$

Differentiation of (10) yields a relation between the uncertainty in longitude $\delta(\Delta\phi)$ and the uncertainty δP in the period

$$\delta(\Delta\phi) = 360°(\Delta t/P^2)\delta P \quad (11)$$

According to (11), for $\delta P = \pm 0.02$ days, a lower limit to the phase coherence time, defined as the time for $\Delta\phi$ to change by ±90°, is 25 years.

Figures 5, 7, and 8 demonstrate that the 27.03-day periodicity and the preferred longitude effect are much more pronounced in the magnetic field than in the solar wind speed. There is no a priori reason that the two parameters should behave identically. V is not proportional to B_r, rather B_r tends to change sign in regions of low V as seen the longitudinal profiles in Figure 3. Furthermore, the longitudinal extent of high-speed streams is less than the extent of a magnetic sector; each sector usually contains both high- and low-speed winds. Another factor is that the solar wind speed is modified by the interaction of fast and slow streams in interplanetary space, while the polarity of the interplanetary field remains unaffected. The greater regularity of the field relative to the speed is also consistent with the contemporary view that the solar magnetic field configuration controls the acceleration of the solar wind. In this respect, the magnetic field is a more fundamental parameter than is the speed.

Our result that the 27.03-day periodicity is much stronger at solar activity maximum than at minimum is perhaps surprising. We tend to think of high-speed recurrent solar wind streams as being a solar minimum phenomenon. Additionally, the geomagnetic *aa* index shows greater 27-day recurrence at solar minimum than at maximum [*Sargent*, 1985]. However, the truth is that the equatorward extensions of the polar coronal holes which are the source of the recurrent high speed streams in the ecliptic occasionally shift their longitudes [e.g., *Hundhausen*, 1977; *Fenimore et al.*, 1978; *Balogh et al.*, 1993; *Macdowall et al.*, 1995; *Mursula and Zieger*, 1996; *Roelof et al.*, 1997]. Furthermore, the in-ecliptic fields are stronger at solar maximum than at minimum, while the passage of an increased number of coronal mass ejections or magnetic clouds at solar maximum does not greatly disturb the underlying magnetic sector pattern [*Smith et al.*, 1986].

It cannot be overemphasized that the 27.03-day periodicity can be discerned only over long periods of time. It is less apparent, or absent, when the data are analyzed for periods of a solar cycle, or a year, or less. For example, the solar cycle plots in Figure 7 show shifts of the 27-day peak to slightly different frequencies and the presence of additional peaks which are not present when the data are considered as a whole. There are several possible explanations for this effect. First, *Gosling and Bame* [1972] suggested that the speed periodicity may be affected by differential rotation with solar latitude; a spacecraft

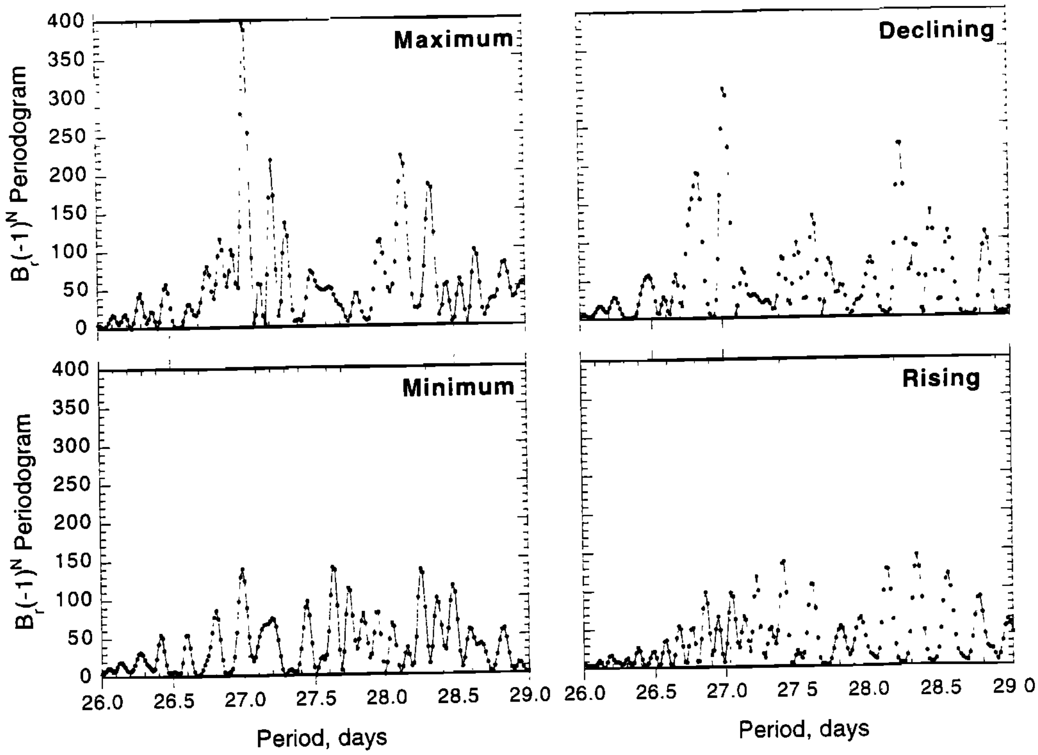

Figure 11. Periodograms of $B_r(-1)^N$ calculated separately for periods of sunspot maximum and minimum and rising and declining activity, as defined in the text.

may sample one period in seasons when it is farthest (±7°) from the heliographic equator and a different one when it is near the equator. Second, abrupt longitudinal jumps by otherwise periodic high-speed streams can lead to additional peaks in a power spectrum [*Fenimore et al.*, 1978]. Finally, power spectra have sidebands on either side of a spectral peak if the signal is modulated in amplitude as well as in frequency, and the magnitudes of both the IMF and the solar wind speed do vary with the phase of the solar cycle. Our results suggest that all these effects are averaged out when a long enough time interval is studied.

In their study of 47 years of IMF polarity variations, *Svalgaard and Wilcox* [1975] found a persistent pattern of rotation periods <27 days during increasing solar activity and periods >27 days during declining activity. A straight line through the phase versus time plot in their Figure 4 yields a 47-year average rotation period of 26.98 days. Although their result is numerically very close to ours, their analysis clearly shows a period <27.00 days. The difference in the two results could arise either from a time variation (there were only 10 years of overlap in the two data sets) or from the difference in the parameters analyzed (sector boundary crossings versus $B_r(-1)^N$).

In Table 4 the rotation period found in this study is compared to rotation periods of some relevant solar phenomena. The rotation periods of coronal holes and coronal magnetic

Table 4. Selected Measurements of Solar Rotation Periods

Measurement	Year	Synodic Period, days	Reference
Solar wind speed and radial IMF	1962-1998	27.03±0.02	this work
Equatorial coronal holes	1972-1973	~27.1	*Krieger* [1977]
Coronal magnetic field	1976-1986		*Hoeksema and Scherrer* [1987]
Northern Hemisphere		26.9	
Southern Hemisphere		28.1	
Photospheric magnetic field at equator	1967-1982	26.91	*Snodgrass* [1983]
Photospheric equatorial dipole	1976-1985	27.0	*Hoeksema and Scherrer* [1987]
Solar envelope	1996 (144 days)		*Schou et al.* [1998]
$0.995\ R_s$		27.32±0.02	
$0.95\ R_s$		26.5	

fields appear to be slightly longer than that of the solar wind, but the time spans of the coronal measurements are not as long as the time spans of the solar wind measurements. The period of the photospheric magnetic field determined by *Snodgrass* [1983] equals 27.03 days at a latitude of ~9°. *Hoeksema and Scherrer* [1987] found a 27.0-day rotation rate for the dipole component of the photospheric magnetic field. Finally, the Michelson Doppler Imager on the SOHO mission has allowed the determination of the solar rotation rate as functions of latitude and distance from the center of the Sun. As shown in Table 4, the equatorial near-surface period is slightly longer than our 27.03 days but decreases to something less than our value only 0.05 solar radii below the surface. A period of 27.03 days can be matched by some combination of increasing the latitude and increasing the depth.

The preferred-longitude behavior found in this study is similar to that seen in stellar observations where an apparent rotational modulation of the calcium emission comes and goes, but when it is present, it usually (but not always) has the same phase (A. H. Vaughan and S. L. Baliunas, unpublished paper presented at IAU Colloquium no. 141, Beijing, China, September 1992). Disk-integrated solar calcium emission also appears to behave in this way (A. Ruzmaikin and J. Feynman, manuscript in preparation, 2000).

Our conclusion is that, on average, and especially at solar maximum, field lines point outward on one side of the Sun and inward on the other, reversing direction in alternate sunspot cycles. The preferred longitude found in this study may be caused by the nonaxisymmetric component of the solar magnetic field ($m = 1$); over short periods of time this component cannot be discerned because of the temporary presence of higher moments. In an alternative view the 27.03-day periodicity may be a state to which the Sun tends to relax, rather than being a permanent phenomenon. In analogy with the geomagnetic field, the solar magnetic pole returns to approximately the same longitude after each reversal. We look forward to seeing whether or not the preferred-longitude phenomena described in this paper persist over the next solar cycle or two.

Acknowledgments. We thank Joyce Wolf for converting the archived Mariner 2 and Pioneer 6 and 7 data to the COHO format and for teaching us about Gaussian random noise. This research was performed at the Jet Propulsion Laboratory of the California Institute of Technology under contract with the National Aeronautics and Space Administration.

Janet G. Luhmann thanks Paul R. Gazis and another referee for their assistance in evaluating this paper.

References

Balogh, A., G. Erdös, R. J. Forsyth, and E. J. Smith, The evolution of the interplanetary sector structure in 1992, *Geophys. Res. Lett., 20*, 2331, 1993.

Bogart, R. S., Recurrence of solar activity: Evidence for active longitudes, *Sol. Phys., 76*, 155, 1982.

Bumba, V., and R. Howard, Solar activity and recurrences in magnetic field distribution, *Sol. Phys., 7*, 28, 1969.

Fenimore, E. E., J. R. Asbridge, S. J. Bame, W. C. Feldman, and J. T. Gosling, The power spectrum of the solar wind speed for periods greater than 10 days, *J. Geophys. Res., 83*, 4353, 1978.

Gonzalez, A. L. C., and W. D. Gonzalez, Periodicities in the interplanetary magnetic field polarity, *J. Geophys. Res., 92*, 4357, 1987.

Gosling, J. T., and S. J. Bame, Solar wind variations 1964-1967: An autocorrelation analysis, *J. Geophys. Res., 77*, 12, 1972.

Gosling, J. T., J. R. Asbridge, S. J. Bame, and W. C. Feldman, Preferred solar wind emitting longitudes on the Sun, *J. Geophys. Res., 82*, 2371, 1977.

Hernandez, G., Time series, periodograms, and significance, *J. Geophys. Res., 104*, 10,355, 1999.

Hoeksema, J. T., and P. H. Scherrer, Rotation of the coronal magnetic field, *Astrophys. J., 318*, 428, 1987.

Horne, J. H., and S. L. Baliunas, A prescription for period analysis of unevenly sampled time series, *Astrophys. J., 302*, 757, 1986.

Hundhausen, A. J., An interplanetary view of coronal holes, in *Coronal Holes and High Speed Wind Streams*, edited by J. B. Zirker, p. 225, Colo. Assoc. Univ. Press, Boulder, 1977.

Krieger, A. S., Temporal behavior of coronal holes, in *Coronal Holes and High Speed Wind Streams*, edited by J. B. Zirker, p. 71, Colo. Assoc. Univ. Press, Boulder, 1977.

Macdowall, R. J., M. D. Desch, M. L. Kaiser, R. G. Stone, R. A. Hess, A. Balogh, S. J. Bame, and B. E. Goldstein, The three-dimensional extent of a high speed solar wind stream, *Space Sci. Rev., 72*, 125, 1995.

Mursula, K., and B. Zieger, The 13.5-day periodicity in the Sun, solar wind, and geomagnetic activity: The last three solar cycles, *J. Geophys. Res., 101*, 27,077, 1996.

Nolte, J. T., and E. C. Roelof, Large-scale structure of the interplanetary medium. I: High coronal source longitude of the quiet-time solar wind, *Solar Phys., 33*, 241, 1973.

Press, W. H., S. A. Teukolsky, W. T. Vetterling, and P. Flannery, *Numerical Recipes in FORTRAN of Scientific Computing*, p. 569, Cambridge Univ. Press, New York, 1992.

Roelof, E. C., G. M. Simnett, R. B. Decker, L. J. Lanzerotti, C. G. Maclennan, T. P. Armstrong, and R. E. Gold, Reappearance of recurrent low-energy particle events at Ulysses/HI-SCALE in the northern hemisphere, *J. Geophys. Res., 102*, 11,251, 1997.

Sargent, H. H., III, Recurrent geomagnetic activity: Evidence for long-lived stability in solar wind structures, *J. Geophys. Res., 90*, 1425, 1985.

Schou, J., et al., Helioseismic studies of differential rotation in the solar envelope by the solar oscillations investigation using the Michelson Doppler imager, *Astrophys. J., 505*, 390, 1998.

Smith, E. J., J. A. Slavin, and B. T. Thomas, The heliospheric current sheet: 3-dimensional structure and solar cycle changes, in *The Sun and Heliosphere in Three Dimensions*, edited by R. G. Marsden, p. 267, D. Reidel, Norwell, Mass., 1986.

Snodgrass, H. B., Magnetic rotation of the solar photosphere, *Astrophys. J., 270*, 288, 1983.

Snyder, C. W., M. Neugebauer, and U. R. Rao, The solar wind velocity and its correlation with cosmic ray variations and with solar and geomagnetic activity, *J. Geophys. Res., 68*, 6361, 1963.

Svalgaard, L., and J. M. Wilcox, Long term evolution of solar sector structure, *Sol. Phys., 41*, 461, 1975.

Trotter, D. E., and D. E. Billings, Longitudinal variations of a zone of solar activity, *Astrophys. J., 136*, 1140, 1962.

Vaughan, A. H., The magnetic activity of sunlike stars, *Science, 225*, 793, 1984.

Vaughan, A. H., S. L. Baliunas, F. Middelkoop, L. Hartmann, D. Mihalas, R. W. Noyes, and G. W. Preston, Stellar rotation in lower main sequence stars measured from time variations in H and K emission line fluxes: Initial results, *Astrophys. J., 250*, 276, 1981.

Wilcox, J. M., and D. S. Colburn, Interplanetary sector structure near the maximum of the sunspot cycle, *J. Geophys. Res., 75*, 6366, 1970.

Wilcox, J. M., and N. F. Ness, Quasi-stationary corotating structure in the interplanetary medium, *J. Geophys. Res., 70*, 5793, 1965.

J. Feynman, M. Neugebauer, A. Ruzmaikin, E. J. Smith, and A. H. Vaughan, MS 169-506, Jet Propulsion Laboratory, California Institute of Technology, 4800 Oak Grove Drive, Pasadena, CA 91109-8099. (mneugeb@jplsp.jpl.nasa.gov)

(Received August 17, 1999; revised October 14, 1999; accepted November 1, 1999)